




## A Bayesian State-Space Approach to Mapping Directional Brain Networks

Huazhang Li, Yaotian Wang, Guofen Yan, Yinge Sun, Seiji Tanabe, Chang-Chia Liu, Mark S. Quigg & Tingting Zhang


To cite this article: Huazhang Li, Yaotian Wang, Guofen Yan, Yinge Sun, Seiji Tanabe, Chang-Chia Liu, Mark S. Quigg & Tingting Zhang (2021) A Bayesian State-Space Approach to Mapping Directional Brain Networks, Journal of the American Statistical Association, 116:536, 1637-1647, DOI: [10.1080/01621459.2020.1865985](https://doi.org/10.1080/01621459.2020.1865985)

To link to this article: <https://doi.org/10.1080/01621459.2020.1865985>

 [View supplementary material](#) 

 Published online: 10 Feb 2021.

 [Submit your article to this journal](#) 

 Article views: 1019

 [View related articles](#) 

 [View Crossmark data](#) 



## A Bayesian State-Space Approach to Mapping Directional Brain Networks

Huazhang Li<sup>\*a</sup>, Yaotian Wang<sup>\*b</sup>, Guofen Yan<sup>c</sup>, Ying Sun<sup>a</sup>, Seiji Tanabe<sup>d</sup>, Chang-Chia Liu<sup>e</sup>, Mark S. Quigg<sup>f</sup>, and Tingting Zhang<sup>b</sup>

<sup>a</sup>Department of Statistics, University of Virginia, Charlottesville, VA; <sup>b</sup>Department of Statistics, University of Pittsburgh, Pittsburgh, PA; <sup>c</sup>Department of Public Health Sciences, University of Virginia, Charlottesville, VA; <sup>d</sup>Department of Psychology, University of Virginia, Charlottesville, VA; <sup>e</sup>Department of Neurosurgery, University of Virginia, Charlottesville, VA; <sup>f</sup>Department of Neurology, University of Virginia, Charlottesville, VA

### ABSTRACT

The human brain is a directional network system of brain regions involving directional connectivity. Seizures are a directional network phenomenon as abnormal neuronal activities start from a seizure onset zone (SOZ) and propagate to otherwise healthy regions. To localize the SOZ of an epileptic patient, clinicians use intracranial electroencephalography (iEEG) to record the patient's intracranial brain activity in many small regions. iEEG data are high-dimensional multivariate time series. We build a state-space multivariate autoregression (SSMAR) for iEEG data to model the underlying directional brain network. To produce scientifically interpretable network results, we incorporate into the SSMAR the scientific knowledge that the underlying brain network tends to have a cluster structure. Specifically, we assign to the SSMAR parameters a stochastic-blockmodel-motivated prior, which reflects the cluster structure. We develop a Bayesian framework to estimate the SSMAR, infer directional connections, and identify clusters for the unobserved network edges. The new method is robust to violations of model assumptions and outperforms existing network methods. By applying the new method to an epileptic patient's iEEG data, we reveal seizure initiation and propagation in the patient's directional brain network and discover a unique directional connectivity property of the SOZ. Overall, the network results obtained in this study bring new insights into epileptic patients' normal and abnormal epileptic brain mechanisms and have the potential to assist neurologists and clinicians in localizing the SOZ—a long-standing research focus in epilepsy diagnosis and treatment. Supplementary materials for this article, including a standardized description of the materials available for reproducing the work, are available as an online supplement.

### ARTICLE HISTORY

Received June 2019  
Accepted December 2020

### KEYWORDS

Cluster structure; Directional connectivity; Intracranial electroencephalography; Stochastic blockmodel

## 1. Introduction

Brain activities form a directional network, where network nodes are brain regions and each network edge represents a directional influence exerted by one region on another. Such directional information flow from one region to another is referred to as directional connectivity also called effective connectivity (Friston 1994). The purposes of this article are to present a new statistical approach for analysis of intracranial electroencephalographic (iEEG) data and to use our approach to uncover the normal and abnormal directional brain networks of epileptic patients over the course of seizure development.

Seizures are a directional network phenomenon (Rosenow and Lüders 2001), as abnormal, excessive, and synchronous neuronal activities start from the seizure onset zone (SOZ) and propagate to otherwise healthy brain regions. Brain surgery to remove the SOZ is a common treatment consideration for patients with drug resistant epilepsy. Presurgical evaluation includes localization of the SOZ using iEEG, which is absolutely critical to the success of the surgery. Clinicians place iEEG electrodes on the exposed brain (inside the skull) of patients with epilepsy to record their neuronal activities in many regions. The recorded data are high-dimensional multivariate time-series of

voltage waveforms, which often exceed 50 channels (with each channel corresponding to one region). Figure 1(a) shows the electrode placement on the left hemisphere of a patient who underwent iEEG recordings in epilepsy evaluation. Figure 1(b) illustrates 5-sec segments of the patient's iEEG recordings in two regions/channels.

To localize the SOZ, trained EEG experts visually examine iEEG waveforms and designate the region that first shows abnormal epileptic activity to be the SOZ (Jacobs et al. 2012). However, despite careful planning, sometimes visual analysis of iEEG fails to localize the SOZ clearly (Harroud et al. 2012). One crucial reason is that sometimes seizure onsets consist of low amplitude, very fast activity. This activity may not generate appropriate power that can be visually detected until the seizure is well underway. Activity with greater power that can be identified may occur later, by which time seizure activity has spread beyond the actual SOZ and involves brain regions that are involved in seizure occurrence but do not serve as the electrical source. Given that seizures are a directional network phenomenon, our method for mapping directional brain networks (i.e., identifying directional connections) using iEEG data is expected to improve understanding of the brain system and localization of the SOZ.

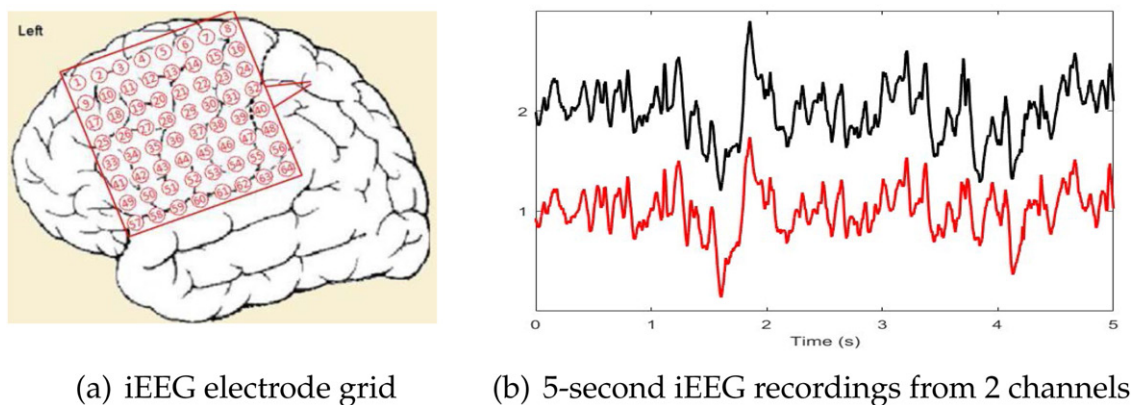


**Figure 1.** (a) The iEEG electrode placement on the left hemisphere of the epileptic patient under study. (b) iEEG time-series segments of two regions/channels.

iEEG data are high-dimensional multivariate time series recordings of many small regions' neuronal activities at a high temporal resolution (millisecond scale) and spatial resolution (about 10 mm in diameter) and with a strong signal-to-noise ratio (SNR) (Cervenka et al. 2013), in contrast to popular functional magnetic resonance imaging (fMRI) with a low temporal resolution and scalp EEG with a low spatial resolution. As such, iEEG data provide valuable information about directional brain networks.

Mapping directional brain networks based on high-dimensional multivariate time series, however, faces multiple challenges. First, it is difficult to construct a model that can accurately characterize the complex mechanism of a high-dimensional brain system, that is, how each region's activity depends on many others' activities. Second, the estimation of a high-dimensional model has a large variance. With many regions being studied and enormous possibilities in directional connections among the regions, it is challenging to identify only a few strong connections among enormous candidate ones. Though incorporating anatomic connectivity (AC) information into the directional connectivity model can improve the estimation of directional connections (Hahn et al. 2019), AC information is not always available. Here, we consider mapping directional brain networks without relying on AC information. Simple sparsity regularization does not address the challenge because high-dimensional sparse networks have many different forms, most of which do not accurately reflect the brain's functional organization. For example, standard  $L_1$ -regularized estimates (Basu and Michailidis 2015; Nicholson, Matteson, and Bien 2017) lead to the sparse network in which every region has only a few connections with other regions. However, this sparse network is not consistent with known brain networks in which regions with similar functions tend to be closely connected (Petersen and Sporns 2015). Third, the computation for analyzing high-dimensional multivariate time series data can be intensive. Existing approaches to mapping directional networks usually address only a part of these challenges, as explained below.

Network mapping approaches fall into two major categories: information-theoretic-measure based methods and model-based methods. The former includes correlations, cross-correlations (Schiff et al. 2005; Kramer, Kolaczyk, and Kirsch 2008), cross-coherence (Schröder and Ombao 2019), transfer

entropy (Vicente et al. 2011), directed transinformation (Hinrichs, Heinze, and Schoenfeld 2006), directed information (Liu and Aviyente 2012), and many others (Wilke, Worrell, and He 2011; van Mierlo et al. 2013). Although these measures are fast to compute, they are mainly for quantifying pairwise relationship between regions and ignore system features of the brain in which each region's activity depends on many other regions' activities. Thus, information-measure-based approaches lack the ability to delineate the entire signal pathway of directional connections from regions to regions.

Model-based methods have been developed to describe simultaneous directional connectivity among all the recorded regions. The most popular models include dynamic causal modeling (DCM, Friston, Harrison, and Penny 2003) and neural mass models (NMM, David and Friston 2003), which use ordinary differential equations (ODE) to characterize directional connectivity. Because of their complex mathematical formulation, the DCM and NNM are typically used for low-dimensional brain networks (consisting of only a few brain regions being studied). To address this limitation, Zhang et al. (2015, 2017, 2019) proposed to use linear ODEs to approximate high-dimensional brain systems (consisting of many regions). However, parameter estimation of deterministic ODE models is sensitive to the model specification, data noise, and data-sampling frequency.

We propose to use a state-space multivariate autoregression-based (SSMAR) model for iEEG data to address the limitation of existing methods. First, the state-space framework allows for separating the model error due to the inherent model inadequacy for a complex system and the data measurement error. The SSMAR with the two errors is flexible to approximate different systems and is robust to various deviations from the assumed model. Equally importantly, the formulation of SSMAR is much simpler than ODE models, which thus, enables fast computation for high-dimensional data.

Different from standard multivariate-autoregression (MAR, Goebel et al. 2003; Harrison, Penny, and Friston 2003; Korzeniewska et al. 2008) and SSMAR (Riera et al. 2004; Cheung et al. 2010), our SSMAR is uniquely constructed for analyzing iEEG data to map directional brain networks. It has been widely documented (Newman 2006; Sporns 2011) that brain networks have a cluster structure, in which regions are more densely connected with regions in the same cluster than with regions otherwise. Our approach incorporates the cluster structure to

greatly improve the model estimation. Specifically, we propose a stochastic blockmodel (SBM)-motivated prior for the SSMAR parameters, restricting the estimated network to have the cluster structure. The SBM (Nowicki and Snijders 2001; Airoldi et al. 2008; Durante and Dunson 2014; Geng, Bhattacharya, and Pati 2019) is a generative model for the networks in the cluster structure. However, existing applications of the SBM (Arroyo-Reli3n et al. 2017; Paul and Chen 2018) and most cluster identification methods (also called community detection, a terminology often used in social network literature) (Goldenberg et al. 2010; Zhao, Levina, and Zhu 2012) are for observed networks with known edges. The proposed method addresses a more challenging problem of inferring *unobserved networks* based on multivariate time series measurements of network nodes' activities.

Using the SBM-motivated prior for SSMAR parameters, we develop a Bayesian framework to make inferences about the underlying network. The proposed Bayesian approach has three major advantages. First, our method improves the efficiency in identifying connected brain regions (i.e., a high true positive) and produces scientifically interpretable network results by incorporating the cluster structure into the model. Second, the proposed Bayesian framework accounts for the model error due to the model inadequacy for the complex system as well as the statistical uncertainty in identifying connected regions. Third, the simple SSMAR formulation brings the flexibility to approximate various brain systems and enables fast computation for high-dimensional multivariate time series data. As such, our approach effectively addresses the three major challenges in mapping high-dimensional brain networks.

The rest of the article is organized as follows. In Section 2, we introduce the new SSMAR model for directional brain networks with the cluster structure. We build a Bayesian hierarchical model with an SBM-motivated prior to make inferences of SSMAR parameters and develop an efficient Markov chain Monte Carlo (MCMC) simulation algorithm for the ensuing posterior inference. In Section 3, we apply the developed Bayesian model to data simulated under two different model settings and network patterns and compare the ensuing results with those of existing network mapping methods. We show that the proposed method is robust to various deviations from the assumed model and outperforms existing methods by achieving much higher accuracy in identifying connected brain regions. Section 4 presents the analysis results of real iEEG data from an epileptic patient by the new SSMAR model. We reveal the patient's directional brain network changes over the course of seizure development, uncover a unique directional connectivity property of the SOZ, and use this property to localize the SOZ. Section 5 concludes with a discussion.

## 2. Dynamic System Models and Bayesian Inference

### 2.1. The State-Space MAR Model

Let  $y(t) = (y_1(t), \dots, y_d(t))'$  be observed iEEG measurements of  $d$  brain regions (equivalently  $d$  network nodes of the brain network under study) at time  $t$  and  $x(t) = (x_1(t), \dots, x_d(t))'$  be the underlying neuronal state functions of the  $d$  brain regions at time  $t$  for  $t = 1, \dots, T$ . Since each iEEG electrode directly records one brain region's neuronal activity with a high spatial

and temporal resolution, we propose a simple space model that links  $y_i(t)$  to  $x_i(t)$ :

$$y_i(t) = c_i \cdot x_i(t) + \epsilon_i(t), \quad i = 1, \dots, d, \quad (1)$$

where  $c_i$  is a unknown constant, and  $\epsilon_i(t)$  is a data measurement error with mean zero.

For the state model that describes directional connectivity among the  $d$  regions at the neuronal level, we propose to use the simplest dynamic system model, that is, the first-order MAR, for  $x(t)$ :

$$x_i(t) = \sum_{j=1}^d A_{ij} \cdot x_j(t-1) + \eta_i(t), \quad i = 1, \dots, d, \quad t = 1, \dots, T,$$

where  $\eta_i(t)$  is the model error due to the model inadequacy in characterizing the dynamics of region  $i$ .

Our goal is to develop a parsimonious model to detect the existence of temporal dependence among neuronal activities of regions rather than building a comprehensive model that can explain all the neuronal activities. Due to the high-dimensionality and the current limited understanding of the brain system, it is extremely difficult to build such a comprehensive dynamic system model. Even though more complex models, such as high-order MARS, may fit the observed data better, they still suffer from the model inadequacy. More seriously, high-order MARS have large estimation errors because they have at least  $d^2$  more parameters than first-order MARS. Consequently, the first-order MAR is more efficient for detecting connected regions and addresses our needs.

Under the SSMAR, identifying connected regions and mapping the brain network are equivalent to selecting statistically significant nonzero  $A_{ij}$ 's. To distinguish nonzero directional connections from zero ones, we introduce indicators for  $A_{ij}$ 's:

$$x_i(t) = \sum_{j=1}^d \gamma_{ij} \cdot A_{ij} \cdot x_j(t-1) + \eta_i(t), \quad i = 1, \dots, d, \quad t = 1, \dots, T, \quad (2)$$

where  $\gamma_{ij}$  is an indicator, taking values either 0 or 1. We use  $\gamma_{ij}$ 's to stand for the set of indicators  $\{\gamma_{ij}, i, j = 1, \dots, d\}$ . The use of indicators is similar to the "spike-and-slab" prior (Miller 2002; Theo and Mike 2004; Ishwaran and Rao 2005) in the Bayesian variable selection framework (George and McCulloch 1993, 1997; Brown, Vannucci, and Fearn 1998; Yi, George, and Allison 2003). Under (2), identifying connected brain regions, that is, selecting directional network edges, is equivalent to selecting nonzero  $\gamma_{ij}$ 's, which is the focus of our model estimation.

The observation model (1) and the state model (2) together are the proposed SSMAR for the brain's directional connectivity. Note that the first-order SSMAR is different from the first-order MAR: The former is robust to violations of model assumptions, but the latter is not. This is because the SSMAR uses two error terms,  $\eta_i(t)$  and  $\epsilon_i(t)$ , to accommodate the model inadequacy and measurement error separately.

We let  $\eta_i(t) \stackrel{iid}{\sim} N(0, 1)$  for several reasons. First,  $c_i$  in (1) and the variance of  $\eta_i(t)$  are not uniquely defined. Since we treat the former as unknown, we fix the latter at 1 to avoid the identifiability issue. Second, letting  $\eta_i(t)$  be independent



between regions enables  $\gamma_{ij}$  and  $A_{ij}$  to capture the dependence between regions more efficiently than otherwise. Third, letting  $\eta_i(t)$  be independent over time brings parsimony to the model. Again, our purpose is to detect the existence of temporal dependence between regions' iEEG rather than capturing all possible temporal dependence. Similarly, for the latter two reasons, we let  $\epsilon_i(t) \stackrel{\text{iid}}{\sim} N(0, \tau_i)$ . We show through simulation studies (Section 3) that our approach is robust to violations of model assumptions.

## 2.2. Bayesian Hierarchical Model for SSMAR

Since nonzero  $\gamma_{ij}$ 's define the brain's directional network, we impose the cluster structure on the estimated brain network through using a SBM-motivated (Fienberg, Meyer, and Wasserman 1985; Nowicki and Snijders 2001; Airoldi et al. 2008; Durante and Dunson 2014) prior for  $\gamma_{ij}$ 's. The cluster structure means that regions within the same cluster connect more closely with each other than with regions in a different cluster. The cluster structure fits the brain's functional organization reported in the literature (Newman 2006; Sporns 2011) and is also useful in epilepsy diagnosis. For example, regions in the SOZ's cluster are those affected by the SOZ's activities most. Information about the SOZ's cluster and its changes during seizure development can help neurologists assess the effect of seizures on brain functions. In summary, developing the SBM-motivated prior for SSMAR parameters to impose the cluster structure on the estimated network is another important novelty of our approach.

Let  $K$  be the prespecified number of clusters. Let  $\mathbf{m}_i = (m_{i1}, \dots, m_{iK})'$  be a  $K$ -dimensional vector with only one element being 1 and the rest being 0;  $\mathbf{m}_i$  labels the cluster of region  $i$ , that is,  $m_{ik} = 1$  indicates region  $i$  in the cluster  $k$ . Let  $B_{k_1 k_2}$ ,  $k_1, k_2 = 1, \dots, K$ , denote the prior probability of a nonzero directional connection from a region in cluster  $k_2$  to another region in cluster  $k_1$ . Let  $\mathbf{B}$  be a  $K \times K$  matrix with entries  $B_{k_1 k_2}$  for  $k_1, k_2 = 1, \dots, K$ .

### 2.2.1. Prior Specification for the Cluster Structure

The prior for the brain network with the cluster structure is a joint distribution for indicators  $\gamma_{ij}$ 's, the cluster labels  $\mathbf{m}_i$ 's, and the probability matrix  $\mathbf{B}$  as follows:

$$\gamma_{ij} | \mathbf{m}_i, \mathbf{m}_j, \mathbf{B} \stackrel{\text{iid}}{\sim} \text{Bernoulli}(\mathbf{m}_i' \mathbf{B} \mathbf{m}_j); \quad (3)$$

$$\mathbf{m}_i \stackrel{\text{iid}}{\sim} \text{Multinomial}(1; p_1, \dots, p_K) \text{ for } i = 1, \dots, d, \text{ and} \\ (p_1, \dots, p_K) \sim \text{Dirichlet}(\boldsymbol{\alpha}); \quad (4)$$

$$B_{kk} \stackrel{\text{iid}}{\sim} \text{Uniform}(l_0, 1) \text{ and } B_{k_1 k_2} \stackrel{\text{iid}}{\sim} \text{Uniform}(0, u_0), \\ k_1, k_2 = 1, \dots, K, k_1 \neq k_2; \quad (5)$$

where  $l_0$  and  $u_0$  are given constants between 0 and 1, and  $\boldsymbol{\alpha} = (1, \dots, 1)$ , assigning uniform weights to different clusters. The distribution (3) specifies the probabilities of both within-cluster and between-cluster connections. For example, if  $m_{ik_1} = 1$  and  $m_{jk_2} = 1$ , then  $\mathbf{m}_i' \mathbf{B} \mathbf{m}_j = B_{k_1 k_2}$ , which is the prior probability of existing a directional connection from cluster  $k_2$  to cluster  $k_1$ ; if  $m_{ik} = 1$  and  $m_{jk} = 1$ ,  $\mathbf{m}_i' \mathbf{B} \mathbf{m}_j = B_{kk}$ , which is the prior probability of existing a directional connection between two regions

in the same cluster  $k$ . Since within-cluster connections are dense and strong, while between-cluster connections are sparse (Park and Friston 2013), we let  $u_0 = 0.1$  and  $l_0 = 0.9$ . The large difference between  $u_0$  and  $l_0$  facilitates differentiating within-cluster connections from between-cluster ones and identifying clusters.

The distributions (3)–(5) together define the SBM-motivated prior for  $\gamma_{ij}$ 's. Our goal is to identify clusters and select significant edges by estimating the cluster labels for regions,  $\mathbf{m}_i$ 's, and the indicators for edges,  $\gamma_{ij}$ 's.

### 2.2.2. Prior Specification for $A_{ij}$ 's

We assign a normal prior to  $A_{ij}$ :

$$A_{ij} \stackrel{\text{iid}}{\sim} N(0, \xi_0^2), \quad (6)$$

where  $\xi_0$  is a positive constant so that the density of  $A_{ij}$  is almost flat within its domain.

### 2.2.3. Priors for Other Parameters

Let  $\mathbf{x}(0) = (x_1(0), \dots, x_d(0))$ ,  $\mathbf{c} = (c_1, \dots, c_d)$ ,  $\boldsymbol{\mu} = (\mu_1, \dots, \mu_d)$ , and  $\boldsymbol{\tau} = (\tau_1, \dots, \tau_d)$ . We assign the following priors to the rest parameters:

$$x_i(0) \stackrel{\text{iid}}{\sim} N(\mu_i, 1), \mu_i \stackrel{\text{iid}}{\sim} N(0, \xi_1^2), c_i \stackrel{\text{iid}}{\sim} N(0, \xi_1^2), \\ p(\tau_i) \propto \frac{1}{\tau_i^{1+\rho_0}} \exp\left\{-\frac{\rho_0}{\tau_i}\right\}, i = 1, \dots, d, \quad (7)$$

where  $\rho_0$  is a prespecified small positive constant to give an almost flat prior for  $\boldsymbol{\tau}$  and  $\xi_1$  is a large positive constant to give almost flat priors for  $c_i$  and  $\mu_i$ .

### 2.2.4. Joint Posterior Distribution

All the parameters to be estimated in the proposed Bayesian framework are  $\Theta = \{\boldsymbol{\Gamma}, \mathbf{B}, \mathbf{M}, \mathbf{A}, \mathbf{c}, \boldsymbol{\tau}, \boldsymbol{\mu}, \mathbf{p}\}$ , where  $\boldsymbol{\Gamma}$  is a  $d \times d$  matrix with entries  $\gamma_{ij}$  for  $i, j = 1, \dots, d$ ,  $\mathbf{M}$  is a  $K \times d$  matrix with the  $i$ th column being  $\mathbf{m}_i$ ,  $\mathbf{A}$  is a  $d \times d$  matrix with entries  $A_{ij}$  for  $i, j = 1, \dots, d$ , and  $\mathbf{p} = \{p_1, \dots, p_K\}$ .

Let  $\mathbf{X} = \{\mathbf{x}(0), \dots, \mathbf{x}(T)\}$  and  $\mathbf{Y} = \{\mathbf{y}(1), \dots, \mathbf{x}(T)\}$ . The SSMAR model (1) and (2) with prior distributions (3)–(7) lead to the posterior distribution:  $p(\mathbf{X}, \Theta | \mathbf{Y}) \propto p(\mathbf{Y} | \mathbf{X}, \Theta) \cdot p(\mathbf{X} | \Theta) \cdot p(\Theta)$ . The detailed formulation of the joint posterior distribution is provided in the Supplementary Appendix.

## 2.3. EM Algorithm for Setting Initial Values and Hyperparameter

We simulate from  $p(\mathbf{X}, \Theta | \mathbf{Y})$  with a partially collapsed Gibbs sampler (Van Dyk and Park 2008), whose MCMC simulation steps are provided in the Supplementary Appendix.

The MCMC simulation can take many iterations to converge especially for large  $d$ . To address this issue, following the practice suggested in Gelman et al. (2013, chap. 13.1), we use an expectation-maximization (EM) algorithm to find the starting values for the MCMC simulation. Specifically, we optimize  $p(\mathbf{Y} | \Theta) = \int p(\mathbf{Y} | \Theta, \mathbf{X}) \cdot p(\mathbf{X} | \Theta) d\mathbf{X}$  by the EM algorithm, in which the state functions  $\mathbf{X}$  are treated as missing values. The output of the EM algorithm,  $\hat{\Theta}$  in the final step, is used as the initial value for the following 10,000 MCMC iterations.

For all our simulation and real data analysis, we verified that the MCMC algorithm converged upon evaluating the Gelman–Rubin statistic Gelman and Rubin (1992).

We need to determine the value of  $K$ , the number of clusters, for the proposed Bayesian model. Standard approaches to selecting hyperparameters for Bayesian methods include information criteria and cross-validation. However, these methods are time-consuming for large  $d$ , because they all require running the posterior simulation for each candidate  $K$ . We propose to select the value for  $K$  by the EM algorithm. Specifically, we let  $K = d$  in our EM algorithm. We set the initial values of  $m_{ii}$  to 1 for  $i = 1, \dots, d$ , that is, we let each region form one independent cluster at the start of the EM algorithm. As the algorithm iterates, several regions fall into the same cluster, and the number of distinct clusters of the  $d$  regions becomes stable. Since the EM algorithm can find the number of clusters that leads to a locally optimal posterior, we let the  $K$  in the Bayesian model be the number of distinct clusters in the final step of the algorithm.

### 2.4. Posterior Inference

We use two posterior probabilities to map the brain network:  $\hat{P}_{ij}^m = \frac{1}{S} \sum_{s=1}^S \delta(\mathbf{m}_i^{(s)}, \mathbf{m}_j^{(s)})$  and  $\hat{P}_{ij}^\gamma = \frac{1}{S} \sum_{s=1}^S \gamma_{ij}^{(s)}$ , where  $S$  is the total number of MCMC samples after burn-in. The former, called the clustering probability, is the posterior probability of two regions  $i$  and  $j$  in the same cluster; and the latter, called the network edge probability, is the posterior probability of nonzero directional connectivity from region  $j$  to  $i$ . We use  $\hat{P}_{ij}^m, i, j = 1, \dots, d$ , to identify clusters. Given a threshold  $\bar{h}^m$ , if  $\hat{P}_{ij}^m > \bar{h}^m$ , regions  $i$  and  $j$  are put in the same cluster; if additionally,  $\hat{P}_{jk}^m > \bar{h}^m$ , then the three regions  $i, j$ , and  $k$  are put in the same cluster regardless of the value of  $\hat{P}_{ik}^m$ . We use  $\hat{P}_{ij}^\gamma$  to select directional network edges. Given a threshold  $\bar{h}^\gamma$ , if  $\hat{P}_{ij}^\gamma > \bar{h}^\gamma$ , we deem the directional connection from region  $j$  to  $i$  nonzero and select the directional network edge from  $j$  to  $i$ .

#### 2.4.1. Choice of Thresholds

The total numbers of potential network edges and possible network patterns are enormous for high-dimensional networks. Because of the uncertainty resulted from the high-dimensionality, posterior probabilities  $\hat{P}_{ij}^m$  and  $\hat{P}_{ij}^\gamma$  are all small. To address this issue, many Bayesian methods select variables based on the ranks of their posterior probabilities (Li et al. 2015; Zhang et al. 2017). We here propose to determine the thresholds for  $\hat{P}_{ij}^m$  and  $\hat{P}_{ij}^\gamma$  based on their significance/ $p$ -values under the null hypothesis that all the regions are independent from each other, as explained in detail below.

We first generate a null dataset  $\mathbf{Y}^0$  that satisfies the null hypothesis. Specifically, given long iEEG time series before seizure onsets, we randomly sample a short segment  $Y_i^0 = \{y_i(t), t = t_i + 1, \dots, t_i + T\}$  of each region  $i$  and let the pairwise distance between any two regions' segments,  $|t_i - t_j|$ , no smaller than  $2T$ . All the regions' segments  $Y_i^0, i = 1, \dots, d$ , form  $\mathbf{Y}^0$ , in which the temporal dependence of each region's time-series data points remains while the dependence between regions' time series is almost none. Applying our Bayesian method to  $\mathbf{Y}^0$ ,

we obtain the ensuing the clustering probabilities and network edge probabilities, which form the empirical null distributions for  $\hat{P}_{ij}^m$ 's and  $\hat{P}_{ij}^\gamma$ 's, respectively. We evaluate the  $p$ -values of  $\hat{P}_{ij}^m$ 's and  $\hat{P}_{ij}^\gamma$ 's based on the null distributions and determine the thresholds for  $\hat{P}_{ij}^m$ 's and  $\hat{P}_{ij}^\gamma$ 's corresponding to the chosen  $p$ -value. We here use the  $p$ -value of 1% to ensure a low false positive rate.

## 3. Simulation Study

### 3.1. Example 1: Simulation From a Third-Order SSMAR

We simulated multivariate time-series data from the following third-order SSMAR.

$$x_i(t) = \sum_{j=1}^d A_{1,ij} x_j(t-1) + \sum_{j=1}^d A_{2,ij} x_j(t-2) + \sum_{j=1}^d A_{3,ij} x_j(t-3) + \eta_i(t) \text{ and}$$

$$y_i(t) = c_i \cdot x_i(t) + \epsilon_i(t).$$

The above system has three clusters of size 15, 15, and 20. We consider region  $j$  has a directional influence over  $i$ , if at least one of  $A_{1,ij}, A_{2,ij}$ , and  $A_{3,ij}$  is nonzero. Figure 2(a) shows the simulated network pattern, where the presence of a directional connection is indicated by an edge (gray edges for within-cluster connections and purple edges for between-cluster connections).

We simulated  $\eta_i(t)$  from the model

$$\eta(t) = 0.5\eta(t-1) + \delta(t) \text{ and } \delta(t) \stackrel{\text{iid}}{\sim} \text{MNV}(0, \Sigma_1), \quad (8)$$

where  $\Sigma_1$  is a block diagonal matrix with each block corresponding to one cluster. The diagonal entries of  $\Sigma_1$  all equal 1 and off-diagonal entries in diagonal submatrices follow  $\text{Uniform}(0, 0.5)$ . The upper bound of off-diagonal entries is chosen such that  $\Sigma_1$  is strictly positive definite.

We generated the observation errors  $\epsilon(t) = (\epsilon_1(t), \dots, \epsilon_d(t))'$  from the model

$$\epsilon(t) = 0.5\epsilon(t-1) + \zeta(t) \text{ and } \zeta(t) \stackrel{\text{iid}}{\sim} \text{MVN}(0, \mathbf{D}^{\frac{1}{2}} \Sigma_2 \mathbf{D}^{\frac{1}{2}}), \quad (9)$$

where  $\Sigma_2$  is created in the same way as  $\Sigma_1$ , and  $\mathbf{D}$  is a  $d$ -by- $d$  diagonal matrix with the diagonal entries chosen such that the SNRs of all the time series equal 10. The median SNR of real iEEG data is much higher than 10 (Zhang et al. 2015). As such, the simulated model errors and data errors are all spatially and temporally correlated, which violates the model assumptions of the proposed SSMAR.

Using the simulated edges as the true values, we calculated false positive rates (FPRs) and true positive rates (TPRs) of network edge selection based on different thresholds for  $\hat{P}_{ij}^\gamma$ 's. For comparison, we examined the FPRs and TPRs of popular competing methods, including the third-order MAR with  $L_1$  regularization (implemented by using the R package BigVAR, Nicholson, Matteson, and Bien 2017), denoted by  $\text{MAR}(L_1)$ , partial directed coherence (PDC, Baccalá and Sameshima 2001), the spectrum synchronicity (Euán, Ombao, and Ortega 2018), and graphical lasso (Glasso, Witten, Friedman, and Simon 2011;

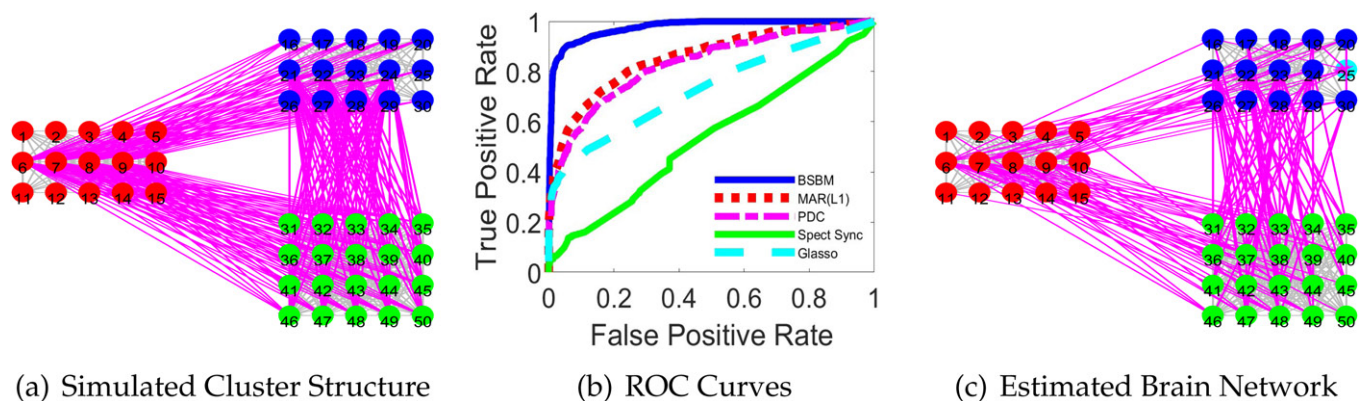


**Figure 2.** (a) The true simulated network structure. (b) The ROC curves of the proposed Bayesian method with a SBM-motivated prior (BSBM) and competing methods including  $MAR(L_1)$ , PDC, the spectrum synchronicity, and Glasso. (c) The estimated network corresponding to 1%  $p$ -value.

Friedman, Hastie, and Tibshirani 2014). Figure 2(b) shows the ROC curves of TPRs versus FPRs for these methods. The proposed Bayesian method with the SBM-motivated prior (BSBM) outperformed the other methods as evidenced by its much greater TPRs given the same FPRs.

Figure 2(c) shows the estimated network pattern using the thresholds corresponding to 1%  $p$ -value for  $\hat{P}_{ij}^m$  and  $\hat{P}_{ij}^y$ . The proposed method was able to identify three clusters. For detecting the directional connections among the 50 regions, the overall TPR and FPR are 0.84 and 0.02. More specifically, the TPR and FPR are 0.95 and 0 for within-cluster connections and 0.45 and 0.02 for between-cluster connections. The comparably low TPR for selecting between-cluster connections is due to several reasons. First, since the clustering is subjective, our selection of directional network edges based on  $P_{ij}^y$  does not account for the identified clusters. As within-cluster connections (accounting for 32.6% of all candidate connections) are much denser than between-cluster connections (9.0% of all candidate connections), network edge selection is more toward selecting within-cluster connections, so that the overall network edge selection accuracy is high. Second, the number of candidate between-cluster connections is enormous and even more than the total number of true network edges. As such, the true between-cluster connections are highly sparse and more difficult to identify than within-cluster connections. Third, since the number of null connections is large, we used a high threshold for  $P_{ij}^y$  to avoid many false selections, which also leads to a low TPR for selecting between-cluster connections. Overall, the proposed method outperformed existing methods by achieving a higher TPR and an almost zero FPR.

In summary, this simulation demonstrates the robustness of our SSMAR to violations of model assumptions and its efficiency in identifying connected regions and clusters.

### 3.2. Example 2: Simulation From the Dynamic Causal Modeling

We simulated time series from a 50-dimension dynamic system given by the DCM (Friston, Harrison, and Penny 2003), the most popular ODE-based model for the brain's directional connectivity. The DCM is for low-dimensional brain networks. We expanded its state model to be high-dimensional and the

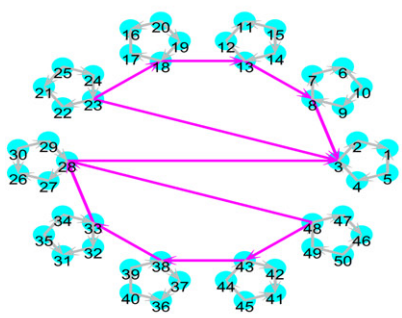
same as that of the sparse regression-DCM (srDCM, Frässle et al. 2018), an extension of the DCM for high-dimensional brain networks. We used this high-dimensional state model to generate  $\mathbf{x}(t)$  of 50 regions. Then we simulated  $\mathbf{y}(t)$  based on the observation model of the DCM, which describes the transformation of neuronal activity  $\mathbf{x}(t)$  into observed  $\mathbf{y}(t)$ . The signal-to-noise was set to be 1, which was considered small in the literature (Frässle et al. 2018). Figure 3(a) shows the simulated directional network among 50 regions.

We applied the proposed BSBM to simulated  $\mathbf{y}(t)$  with 2714 time points, which were identical to those of the simulated data under the srDCM (Frässle et al. 2018). We also applied the BSBM to down-sampled data with 1000 time points. Figures 3(b) and (c) show the ROC curves of the BSBM and other competing methods for the data of two frequencies. We also analyzed the simulated data using the srDCM. Though the proposed SSMAR is distinct from the DCM and srDCM, our method was robust to model specification, data noise, and data-sampling frequency and outperformed existing methods by achieving the largest area under the ROC curve.

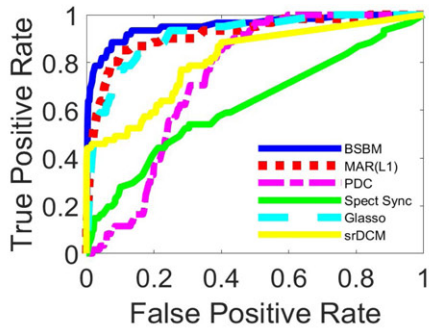
## 4. Real iEEG Data Analysis

We applied the proposed method to iEEG data of a patient with epilepsy, who had 64 electrodes placed on the exposed surface of his brain, as shown in Figure 1(a). iEEG recorded the patient's brain activities in three seizures. The sampling rate of this patient's iEEG data was 4000 Hz. We down-sampled the iEEG data to 1000 Hz, a typical rate used in the literature (Burns et al. 2014; Zhang et al. 2015). EEG experts manually examined the data and determined seizure onset times and the SOZ, which was G37. A responsive neurostimulation system was later implanted in his brain with a lead placed on G37. The use of RNS has significantly reduced his seizure occurrences. This confirms that the SOZ was accurately located. In our analysis, we treated seizure onset times as given, since the detection of seizure onset time is not difficult. However, we did not use the location information of the SOZ when mapping the directional brain network among recorded brain sites. The SOZ was treated as unknown and equally as other brain sites. As such, we could validate our network results against the location information of the SOZ.

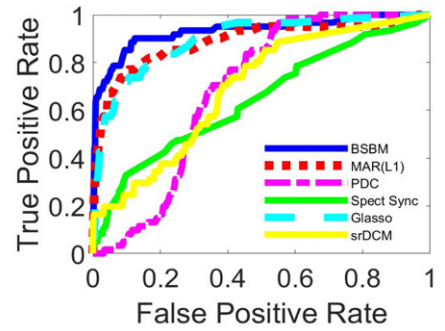




(a) Simulated Network

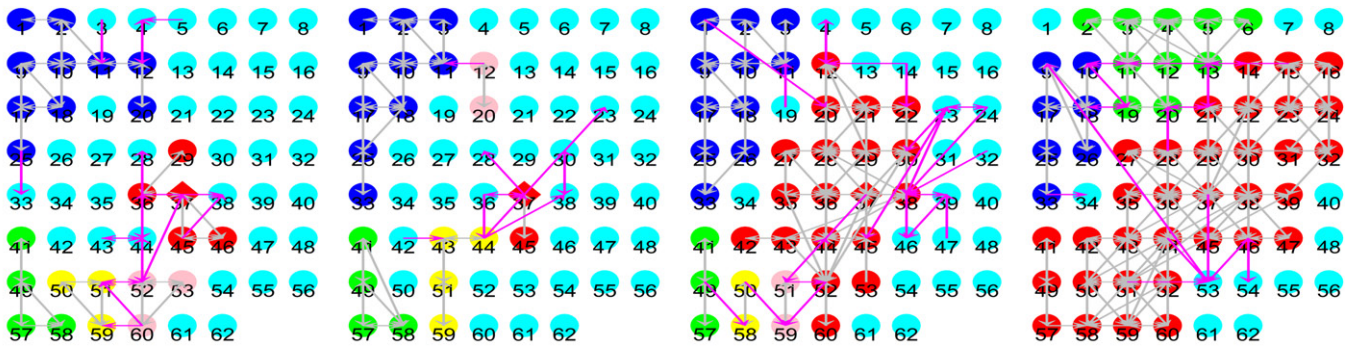


(b) ROC Curves for Data with 2714 Time Points



(c) ROC Curves for Data with 1000 Time Points

**Figure 3.** Simulation studies of two generative models for fMRI data. (a) The simulated (true) network pattern. (b) ROC curves of network edges selection for the simulated data at 2714 time points. (c) ROC curves of network edge selection for the simulated data at 1000 time points.



(a)  $t \in [-50, -25]$  sec-onds (b)  $t \in [-25, 0]$  seconds (c)  $t \in [0, 25]$  seconds (d)  $t \in [25, 50]$  seconds

**Figure 4.** Brain networks for four periods.  $t = 0$  is the starting time of seizure onset. Gray and purple edges indicate within-cluster and between-cluster directional connections, respectively, based on a threshold corresponding to 1%  $p$ -value. The node in the diamond is G37, the true SOZ. A node in light blue corresponds to a region in a cluster containing itself only. Nodes in the same color (dark blue, green, pink, red, or yellow) are regions identified to be in the same cluster.

Channels 63 and 64, as the reference electrodes, were removed from the analysis. We evaluated connectivity among the rest 62 regions. To minimize the residual artifacts of 60 Hz electrical noise, we used a 60 Hz notch filter during the primary recording and removed the first principal component through the principal component analysis.

Once a seizure starts, the connection strength between the SOZ and other regions increases (Englot, Konrad, and Morgan 2016), resulting in abnormally synchronized or excessive neuronal activities in other regions (Fisher et al. 2014). Thus, an effective brain network mapping methods should reveal different brain networks before and after seizure onset: More regions are expected to be affected by the activities from the SOZ after the seizure onset. We applied our method to map brain networks in the periods around the seizure onset time and examined the effectiveness of our method in revealing different brain networks before and after seizure onset. We focused on four time periods: 26–50 sec before seizure onset, 1–25 sec before seizure onset, 1–25 sec after seizure onset, and 26–50 sec after seizure onset. To ensure effective approximation of the underlying complex brain system by the SSMAR and also to accommodate potential variation of brain activities over time, we applied the developed method to each 1-sec iEEG segment (containing 1000 time series measurements) independently. In

total, we analyzed 300 1-sec iEEG data segments (4 periods  $\times$  25 sec  $\times$  3 seizures).

For each 1-sec data segment and for each pair of regions  $i$  and  $j$ , we obtained their clustering probability  $\hat{P}_{ij}^m$  and network edge probabilities  $\hat{P}_{ij}^\gamma$  and  $\hat{P}_{ji}^\gamma$ . For each seizure period, we took average of posterior probabilities in 75 segments and denoted the ensuing average posterior probabilities by  $\bar{P}_{ij}^m$ ,  $\bar{P}_{ij}^\gamma$ , and  $\bar{P}_{ji}^\gamma$ . We identified clusters and connected brain regions and mapped brain networks for four seizure periods based on these average probabilities. This analysis is consistent with the medical practice where reliable epilepsy diagnosis is based on combined information of iEEG recordings of at least three seizures (Marks and Laxer 1998).

### 4.1. Network Results

Figures 4(a)–(d) show estimated networks for the four periods using the thresholds corresponding to the  $p$ -value of 1%. The SOZ is at G37, indicated by the diamond in all these four figures, while all the other regions are indicated by circles. The shown network edges (in gray or purple) indicate their network edge probabilities above the threshold; and the nodes indicated by the same color (other than light blue) are corresponding to the regions



identified to be in the same cluster. Each region indicated by light blue forms one cluster that contains the region itself only.

Our method reveals that the networks for the two pre-seizure periods were similar (Figures 4(a) and (b)), indicating that the subject's brain network was steady before seizure onset. However, dramatic changes occurred in the networks once seizure started (Figures 4(c) and (d)). Compared to the pre-seizure networks, more regions were connected to the SOZ (G37) and fell into the same cluster as the SOZ, indicating that the activity of the SOZ affected more and more regions as seizure developed. This result is in line with the existing understanding of seizure propagation (Rosenow and Lüders 2001; Englot, Konrad, and Morgan 2016).

To demonstrate the advantages of our method, we also analyzed the same iEEG data using several competing methods, including correlation, cross-correlation, PDC (Baccalá and Sameshima 2001), directed transfer function (DTF, Kaminski and Blinowska 1991),  $L_1$ -penalized MAR (MAR( $L_1$ )), and Glasso (Witten, Friedman, and Simon 2011; Friedman, Hastie, and Tibshirani 2014). We used each of these methods to analyze 300 1-sec segments independently and obtained 300 calculated values for each candidate network edge (either directional or

undirectional depending on the method). For each candidate network edge, we used the average of 75 values in each period to quantify the strength of connection. For comparison, we selected network edges with top 5% averages, because the network edges selected by our method based on the  $p$ -value of 1% roughly correspond to the edges with top 5%  $\bar{P}_{ij}^V$ 's. Figures 5(a)–(l) show the networks estimated by the competing methods in the periods right before and right after the seizure onset. All these popular methods failed to detect the changes in the network at the seizure onset time, as evidenced by the similarity between the pre-onset and seizure-onset networks.

#### 4.2. SOZ Localization

We hypothesize that the SOZ exhibits a significant change in its connectivity to other regions at the seizure onset. To quantify this change, we developed the following method. For each period, for each region, say  $j$ , we calculated the average of network edge probabilities from  $j$  to all the other regions,  $\sum_i \bar{P}_{ij}^V/d$ , referred to as region  $j$ 's average directional connectivity (ADC) in the period. We use the ADC difference between the periods

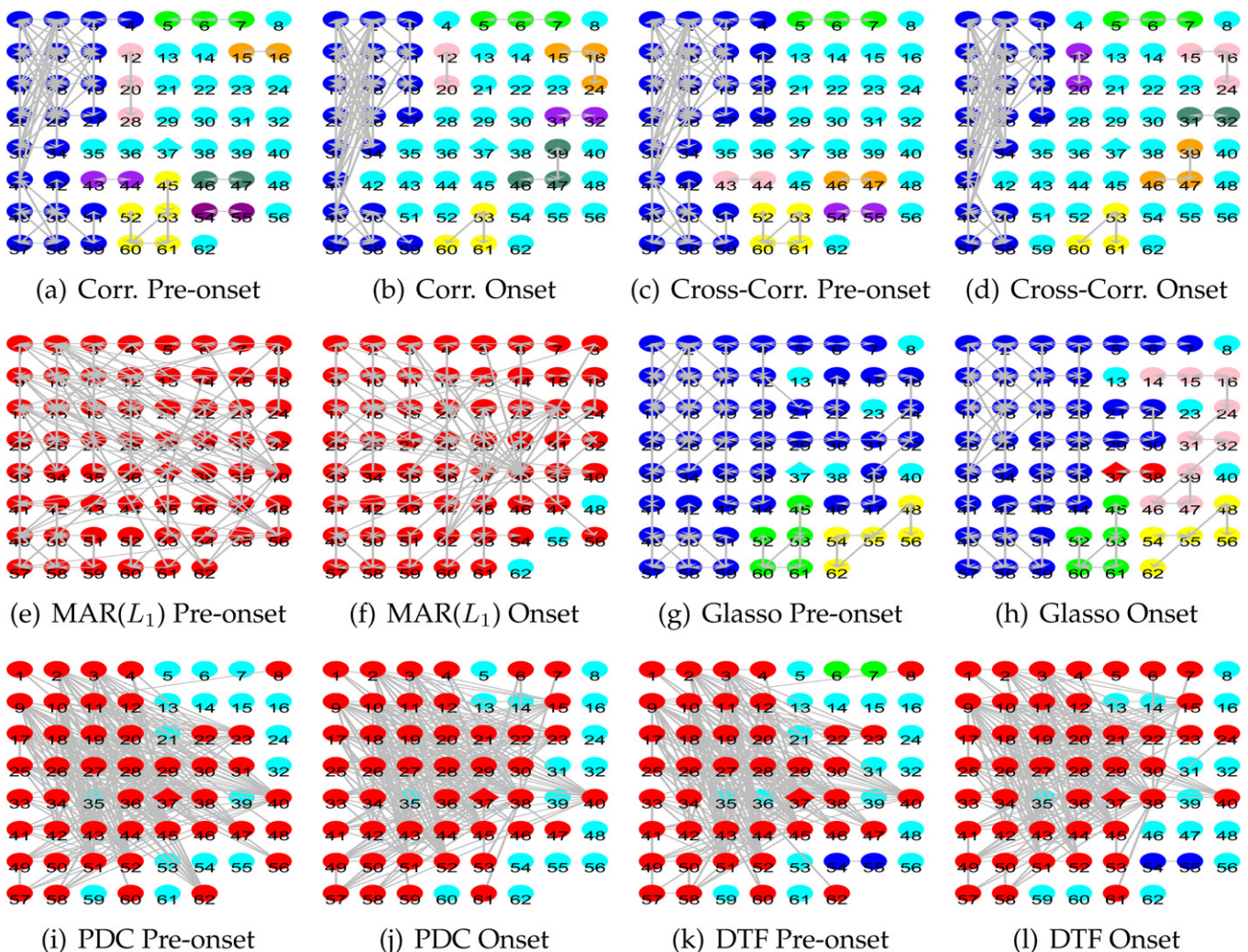


Figure 5. Brain networks estimated using correlation, cross-correlation, MAR with an  $L_1$  penalty (MAR( $L_1$ )), graphical Lasso (Glasso), partial directed coherence (PDC), and directed transfer function (DTF) methods. Each network edge indicates a pair of regions identified to be connected by the competing methods.

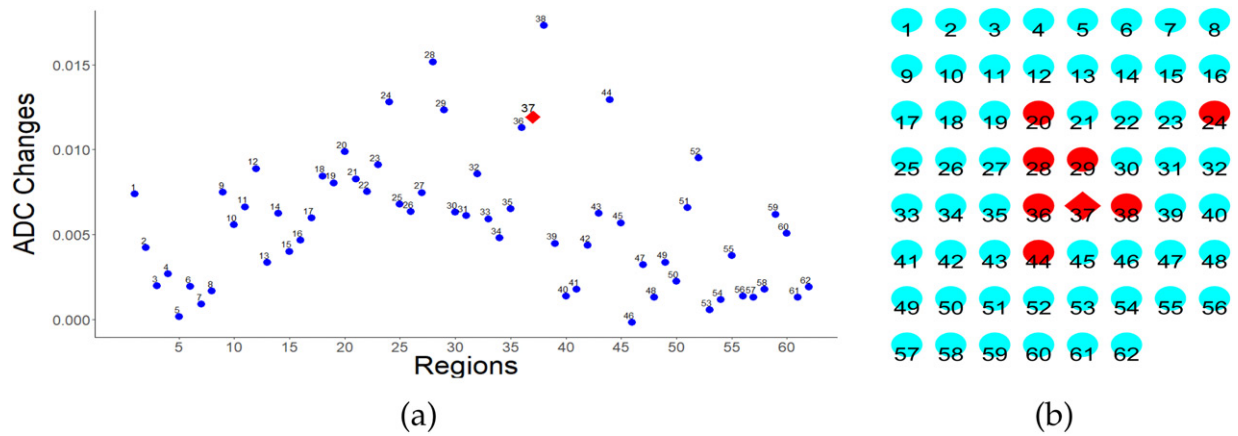


Figure 6. (a) Directional connectivity changes of 62 regions at seizure onset. (b) Regions with highest increases in directional connectivity.

right after and before the seizure onset to quantify the change in directional connectivity from region  $j$  to other regions. Figure 6 shows the ADC changes of 62 regions at the seizure onset. Except for one region, the SOZ and its neighboring regions have the highest increases in ADC.

We propose to select the regions with high ADC increases to be candidates for SOZ. To determine the threshold for ADCs, we calculated the 62 regions’ ADC changes in the first two pre-seizure periods for the three seizures recorded by iEEG. Then we selected the regions whose ADC changes at the seizure onset are larger than the maximum of ADC changes in the two pre-seizure periods. Figure 6(b) shows the selected regions (in red).

Our result showed that the small brain area including the SOZ G37 has the highest increase in directional connectivity at the seizure onset. This result is in line with the existing literature about the SOZ (Englot, Konrad, and Morgan 2016): the abnormal, excessive neuronal activity starts from it and spreads to other regions. Our method quantified brain network changes and uncovered that the brain area including the SOZ first demonstrated an increase in directional connectivity during the seizure development.

In summary, with our method, we revealed three characteristics of the epileptic patient’s directional brain network. (1) The patient’s network changed at the seizure onset time. (2) The change occurred around the SOZ, as the SOZ cluster expanded to include more regions, and the number of directional connections between the SOZ and other regions increased. (3) The extent of the directional connectivity of the SOZ increased most compared to other regions at the seizure onset time. These three results are in line with the existing understanding of seizure initiation and propagation. In contrast, existing network methods could not obtain the above three results together. These results are useful for identifying the brain areas affected by seizures and for evaluating the effect of seizures on brain functions. Also, our method has the potential to help clinicians localize the SOZ and, thus, to improve epilepsy diagnosis and treatment.

### 5. Discussion

This article develops a new high-dimensional dynamic system model for mapping directional brain networks using iEEG data.

The proposed approach has three novelties. First, the proposed state-space first-order MAR-based model for the brain network is effective for approximating various high-dimensional brain systems. The model is robust to violations of model assumptions. Second, in contrast to standard SSMAR and MAR models, the proposed Bayesian framework incorporates the prior knowledge of the cluster structure into the model estimation, which addresses the challenge in detecting connected brain regions among many possible ones. Our method produces scientifically meaningful network results. Third, we develop a stochastic-blockmodel (SBM)-motivated prior to impose the cluster structure on the SSMAR parameters that denote directional edges. This is novel from standard SBMs for observed networks where network edges are directly known.

The proposed method can robustly detect directional connections with high accuracy, even if the underlying model for the brain network is nonlinear for three reasons. First, we apply the SSMAR to short iEEG time segments so that the linear model can effectively approximate the underlying network system. Second, we use the proposed model to identify the directional connections through detecting the existence of temporal dependence among neuronal activities of regions rather than estimating the nonlinear interactions among regions. The first-order SSMAR focuses only on the primary temporal dependence (rather than the exact order or nonlinearity of the dependence) among multivariate time series. Thus, the model is parsimonious in terms of the number of model parameters and enables efficient detection of directional connections among many regions. Third, the SBM-motivated prior can effectively capture potential brain network patterns. Using the SBM-motivated prior increases the efficiency in detecting directional connections. In summary, the proposed integration of a conventional SSMAR and the cluster structure yields robustness, flexibility, efficiency, and computational feasibility in modeling and estimating brain network systems.

The obtained network results from iEEG data analysis by the proposed method reveal how seizures propagate from the SOZ to other regions and thus, bring new insights into the brain’s normal and abnormal mechanisms and functions and dysfunctions. By assuming the cluster structure for the brain network, we identify the SOZ’s cluster (the regions affected strongly by the SOZ’s activity) and its changes during seizure



development. Such information can help neurologists assess the effect of seizures on brain functions. Moreover, by revealing the unique connectivity property of the SOZ, our network analysis can improve SOZ localization in clinical treatment for epilepsy.

We have applied statistical methods used for localizing the SOZ based on EEG data to our iEEG data. Specifically, Schröder and Ombao (2019) developed frequency specific methods to localize the SOZ through detecting changes in EEG data; and Wang, Ombao, and Chung (2018) used the differences in persistent homology between EEG data in pre-seizure and seizure periods to localize the SOZ. However, these methods tend to have much higher FPRs than the proposed method most likely because EEG and iEEG data have different properties. The two methods (Wang, Ombao, and Chung 2018; Schröder and Ombao 2019) require the time series before and after seizures to be stationary for a relatively long period. Since the regions recorded by EEG are large and spatially distant from each other, the changes in one EEG region take a relatively long time to spread to other regions. As such, the assumption of stationary long time series required by the two methods can be satisfied with EEG data. In contrast, regions recorded by iEEG are spatially close. Seizures propagate from the SOZ to other regions quickly, and thus, many regions surrounding the SOZ can have sharp changes in frequencies and persistent homology in a short period of time. This phenomenon makes it difficult for the methods that rely on relatively long stationary time series to separate the SOZ from surrounding regions. Because our method is focused on detecting the change in directional connectivity instead of the change in time series, our method can better exclude non-SOZ regions whose directional connectivity remains unchanged at the seizure onset.

## Supplementary Materials

The supplementary materials provide details of posterior inferences of the proposed Bayesian method.

## Funding

Tingting Zhang gratefully acknowledges the support by NSF-1758095.

## References

- Airoldi, E. M., Blei, D. M., Fienberg, S. E., and Xing, E. P. (2008), "Mixed Membership Stochastic Blockmodels," *Journal of Machine Learning Research*, 9, 1981–2014. [1639,1640]
- Arroyo-Relión, J. D., Kessler, D., Levina, E., and Taylor, S. F. (2017), "Network Classification With Applications to Brain Connectomics," arXiv no. 1701.08140. [1639]
- Baccalá, L. A., and Sameshima, K. (2001), "Partial Directed Coherence: A New Concept in Neural Structure Determination," *Biological Cybernetics*, 84, 463–474. [1641,1644]
- Basu, S., and Michailidis, G. (2015), "Regularized Estimation in Sparse High-Dimensional Time Series Models," *The Annals of Statistics*, 43, 1535–1567. [1638]
- Brown, P. J., Vannucci, M., and Fearn, T. (1998), "Multivariate Bayesian Variable Selection and Prediction," *Journal of the Royal Statistical Society, Series B*, 60, 627–641. [1639]
- Burns, S. P., Santaniello, S., Yaffe, R. B., Jouny, C., Crone, N., Bergey, G., Anderson, W. S., and Sarma, S. V. (2014), "Network Dynamics of the Brain and Influence of the Epileptic Seizure Onset Zone," *Proceedings of the National Academy of Sciences of the United States of America*, 111, 5321–5330. [1642]
- Cervenka, M. C., Franaszczuk, P. J., Crone, N. E., Hong, B., Caffo, B., Bhatt, P., Lenz, F. A., and Boatman-Reich, D. (2013), "Reliability of Early Cortical Auditory Gamma-Band Responses," *Clinical Neurophysiology*, 124, 70–82. [1638]
- Cheung, B. L., Riedner, B. A., Tononi, G., and Van Veen, B. D. (2010), "Estimation of Cortical Connectivity From EEG Using State-Space Models," *IEEE Transactions on Biomedical Engineering*, 57, 2122–2134. [1638]
- David, O., and Friston, K. J. (2003), "A Neural Mass Model for MEG/EEG: Coupling and Neuronal Dynamics," *NeuroImage*, 20, 1743–1755. [1638]
- Durante, D., and Dunson, D. B. (2014), "Nonparametric Bayes Dynamic Modelling of Relational Data," *Biometrika*, 101, 883–898. [1639,1640]
- Englot, D. J., Konrad, P. E., and Morgan, V. L. (2016), "Regional and Global Connectivity Disturbances in Focal Epilepsy, Related Neurocognitive Sequelae, and Potential Mechanistic Underpinnings," *Epilepsia*, 57, 1546–1557. [1643,1644,1645]
- Euán, C., Ombao, H., and Ortega, J. (2018), "Spectral Synchronicity in Brain Signals," *Statistics in Medicine*, 37, 2855–2873. [1641]
- Fienberg, S. E., Meyer, M. M., and Wasserman, S. S. (1985), "Statistical Analysis of Multiple Sociometric Relations," *Journal of the American Statistical Association*, 80, 51–67. [1640]
- Fisher, R. S., Acevedo, C., Arzimanoglou, A., Bogacz, A., Cross, J. H., Elger, C. E., Engel, J., Jr., Forsgren, L., French, J. A., Glynn, M., and Hesdorffer, D. C. (2014), "ILAE Official Report: A Practical Clinical Definition of Epilepsy," *Epilepsia*, 55, 475–482. [1643]
- Frässle, S., Lomakina, E. I., Kasper, L., Manjaly, Z. M., Leff, A., Pruessmann, K. P., Buhmann, J. M., and Stephan, K. E. (2018), "A Generative Model of Whole-Brain Effective Connectivity," *Neuroimage*, 179, 505–529. [1642]
- Friedman, J., Hastie, T., and Tibshirani, R. (2014), "glasso: Graphical Lasso-Estimation of Gaussian Graphical Models," R Package Version 1. [1642,1644]
- Friston, K. J. (1994), "Functional and Effective Connectivity in Neuroimaging: A Synthesis," *Human Brain Mapping*, 2, 56–78. [1637]
- Friston, K. J., Harrison, L., and Penny, W. D. (2003), "Dynamic Causal Modelling," *NeuroImage*, 19, 1273–1302. [1638,1642]
- Gelman, A., and Rubin, D. B. (1992), "Inference From Iterative Simulation Using Multiple Sequences," *Statistical Science*, 7, 457–511. [1641]
- Gelman, A., Stern, H. S., Carlin, J. B., Dunson, D. B., Vehtari, A., and Rubin, D. B. (2013), *Bayesian Data Analysis*, Boca Raton, FL: Chapman and Hall/CRC. [1640]
- Geng, J., Bhattacharya, A., and Pati, D. (2019), "Probabilistic Community Detection With Unknown Number of Communities," *Journal of the American Statistical Association*, 114, 893–905. [1639]
- George, E. I., and McCulloch, R. E. (1993), "Variable Selection via Gibbs Sampling," *Journal of the American Statistical Association*, 88, 881–889. [1639]
- (1997), "Approaches for Bayesian Variable Selection," *Statistica Sinica*, 7, 339–373. [1639]
- Goebel, R., Roebroeck, A., Kim, D.-S., and Formisano, E. (2003), "Investigating Directed Cortical Interactions in Time-Resolved fMRI Data Using Vector Autoregressive Modeling and Granger Causality Mapping," *Magnetic Resonance Imaging*, 21, 1251–1261. [1638]
- Goldenberg, A., Zheng, A. X., Fienberg, S. E., and Airoldi, E. M. (2010), "A Survey of Statistical Network Models," *Foundations and Trends in Machine Learning*, 2, 129–233. [1639]
- Hahn, G., Skeide, M. A., Mantini, D., Ganzetti, M., Destexhe, A., Friederici, A. D., and Deco, G. (2019), "A New Computational Approach to Estimate Whole-Brain Effective Connectivity From Functional and Structural MRI, Applied to Language Development," *Scientific Reports*, 9, 8479. [1638]
- Harrison, L., Penny, W. D., and Friston, K. (2003), "Multivariate Autoregressive Modeling of fMRI Time Series," *Neuroimage*, 19, 1477–1491. [1638]
- Harroud, A., Bouthillier, A., Weil, A. G., and Nguyen, D. K. (2012), "Temporal Lobe Epilepsy Surgery Failures: A Review," *Epilepsy Research and Treatment*, 2012, 201651. [1637]
- Hinrichs, H., Heinze, H. J., and Schoenfeld, M. A. (2006), "Causal Visual Interactions as Revealed by an Information Theoretic Measure and fMRI," *Neuroimage*, 31, 1051–1060. [1638]



- Ishwaran, H., and Rao, J. S. (2005), "Spike and Slab Variable Selection: Frequentist and Bayesian Strategies," *The Annals of Statistics*, 33, 730–773. [1639]
- Jacobs, J., Staba, R., Asano, E., Otsubo, H., Wu, J. Y., Zijlmans, M., Mohamed, I., Kahane, P., Dubeau, F., Navarro, V., and Gotman, J. (2012), "High-Frequency Oscillations (HFOs) in Clinical Epilepsy," *Progress in Neurobiology*, 98, 302–315. [1637]
- Kaminski, M., and Blinowska, K. J. (1991), "A New Method of the Description of the Information Flow in the Brain Structures," *Biological Cybernetics*, 65, 203–210. [1644]
- Korzeniewska, A., Crainiceanu, C. M., Kuś, R., Franaszczuk, P. J., and Crone, N. E. (2008), "Dynamics of Event-Related Causality in Brain Electrical Activity," *Human Brain Mapping*, 29, 1170–1192. [1638]
- Kramer, M. A., Kolaczuk, E. D., and Kirsch, H. E. (2008), "Emergent Network Topology at Seizure Onset in Humans," *Epilepsy Research*, 79, 173–186. [1638]
- Li, F., Zhang, T., Wang, Q., Gonzalez, M. Z., Maresh, E. L., and Coan, J. A. (2015), "Spatial Bayesian Variable Selection and Grouping in High-Dimensional Covariate Spaces With Application to fMRI," *The Annals of Applied Statistics*, 9, 687–713. [1641]
- Liu, Y., and Aviyente, S. (2012), "Quantification of Effective Connectivity in the Brain Using a Measure of Directed Information," *Computational and Mathematical Methods in Medicine*, 2012, 635103. [1638]
- Marks, W. J., Jr., and Laxer, K. D. (1998), "Semiology of Temporal Lobe Seizures: Value in Lateralizing the Seizure Focus," *Epilepsia*, 39, 721–726. [1643]
- Miller, A. (2002), *Subset Selection in Regression*, Boca Raton, FL: CRC Press. [1639]
- Newman, M. E. J. (2006), "Modularity and Community Structure in Networks," *Proceedings of the National Academy of Sciences of the United States of America*, 103, 8577–8696. [1638,1640]
- Nicholson, W. B., Matteson, D. S., and Bien, J. (2017), "VARX-L: Structured Regularization for Large Vector Autoregressions With Exogenous Variables," *International Journal of Forecasting*, 33, 627–651. [1638,1641]
- Nowicki, K., and Snijders, T. A. B. (2001), "Estimation and Prediction for Stochastic Blockstructures," *Journal of the American Statistical Association*, 96, 1077–1087. [1639,1640]
- Park, H.-J., and Friston, K. (2013), "Structural and Functional Brain Networks: From Connections to Cognition," *Science*, 342, 1238411, DOI: doi: 10.1126/science.1238411. [1640]
- Paul, S., and Chen, Y. (2018), "A Random Effects Stochastic Block Model for Joint Community Detection in Multiple Networks With Applications to Neuroimaging," arXiv no. 1805.02292. [1639]
- Petersen, S. E., and Sporns, O. (2015), "Brain Networks and Cognitive Architectures," *Neuron*, 88, 207–219. [1638]
- Riera, J. J., Watanabe, J., Kazuki, I., Naoki, M., Aubert, E., Ozaki, T., and Kawashima, R. (2004), "A State-Space Model of the Hemodynamic Approach: Nonlinear Filtering of Bold Signals," *NeuroImage*, 21, 547–567. [1638]
- Rosenow, F., and Lüders, H. (2001), "Presurgical Evaluation of Epilepsy," *Brain*, 124, 1683–1700. [1637,1644]
- Schiff, S. J., Sauer, T., Kumar, R., and Weinstein, S. L. (2005), "Neuronal Spatiotemporal Pattern Discrimination: The Dynamical Evolution of Seizures," *NeuroImage*, 28, 1043–1055. [1638]
- Schröder, A. L., and Ombao, H. (2019), "FreSpeD: Frequency-Specific Change-Point Detection in Epileptic Seizure Multi-Channel EEG Data," *Journal of the American Statistical Association*, 114, 115–128. [1638,1646]
- Sporns, O. (2011), *Networks of the Brain*, Cambridge, MA: The MIT Press. [1638,1640]
- Theo, H. E. and Mike, E. G. (2004), "Mapping Multiple QTL Using Linkage Disequilibrium and Linkage Analysis Information and Multitrait Data," *Genetics Selection Evolution*, 36, 261–279. [1639]
- Van Dyk, D. A., and Park, T. (2008), "Partially Collapsed Gibbs Samplers: Theory and Methods," *Journal of the American Statistical Association*, 103, 790–796. [1640]
- van Mierlo, P., Carrette, E., Hallez, H., Raedt, R., Meurs, A., Vandenberghe, S., Van Roost, D., Boon, P., Staelens, S., and Vonck, K. (2013), "Ictal-Onset Localization Through Connectivity Analysis of Intracranial EEG Signals in Patients With Refractory Epilepsy," *Epilepsia*, 54, 1409–1418. [1638]
- Vicente, R., Wibral, M., Lindner, M., and Pipa, G. (2011), "Transfer Entropy—A Model-Free Measure of Effective Connectivity for the Neurosciences," *Journal of Computational Neuroscience*, 30, 45–67. [1638]
- Wang, Y., Ombao, H., and Chung, M. K. (2018), "Topological Data Analysis of Single-Trial Electroencephalographic Signals," *The Annals of Applied Statistics*, 12, 1506. [1646]
- Wilke, C., Worrell, G., and He, B. (2011), "Graph Analysis of Epileptogenic Networks in Human Partial Epilepsy," *Epilepsia*, 52, 84–93. [1638]
- Witten, D. M., Friedman, J. H., and Simon, N. (2011), "New Insights and Faster Computations for the Graphical Lasso," *Journal of Computational and Graphical Statistics*, 20, 892–900. [1641,1644]
- Yi, N., George, V., and Allison, D. B. (2003), "Stochastic Search Variable Selection for Identifying Multiple Quantitative Trait Loci," *Genetics*, 164, 1129–1138. [1639]
- Zhang, T., Sun, Y., Yan, G., Yin, Q., Li, H., Tanabe, S., Caffo, B., and Quigg, M. (2019), "Bayesian Inference of a Directional Brain Network for Intracranial EEG Data," *Computational Statistics and Data Analysis* (under review). [1638]
- Zhang, T., Wu, J., Li, F., Caffo, B., and Boatman-Reich, D. (2015), "A Dynamic Directional Model for Effective Brain Connectivity Using Electroencephalographic (EEG) Time Series," *Journal of the American Statistical Association*, 110, 93–106. [1638,1641,1642]
- Zhang, T., Yin, Q., Caffo, B., Sun, Y., and Boatman-Reich, D. (2017), "Bayesian Inference of High-Dimensional, Cluster-Structured Ordinary Differential Equation Models With Applications to Brain Connectivity Studies," *The Annals of Applied Statistics*, 11, 868–897. [1638,1641]
- Zhao, Y., Levina, E., and Zhu, J. (2012), "Consistency of Community Detection in Networks Under Degree-Corrected Stochastic Block Models," *The Annals of Statistics*, 40, 2266–2292. [1639]